Designing and Testing Liquid Engines for Additive Manufacturing

Deepak M. Atyam[1] and Ngoc H. Nguyen[2]
University of California, San Diego, La Jolla, CA, 92093

The SEDS UCSD's (Students for the Exploration and Development of Space Chapter at the University of California, San Diego) development of their second additively manufactured rocket engine, Ignus is presented. The purpose of this project is to research the feasibility of additively manufactured rocket engines in order to pave the way for larger and more powerful engines that are to be additively manufactured in hopes of providing easier access to space. By utilizing additive manufacturing, we have proven that dynamic pressures can be utilized instead of static pressures as a new manifolding technique. The design process for the Ignus engine is explained and justified through calculations and illustrations. Ultimately, the aim is to prove that utilizing the benefits of additively manufacturing rocket engines will provide a significant reduction in time and weight when compared to traditional rocket engine fabrication, as seen through the development and future testing of Ignus.

Nomenclature

Δp	=	Coolant pressure drop through the portion of cooling passage under consideration, lb/in^2
L	=	Length of that portion, in
d	=	Equivalent average diameter of that portion, in
ρ	=	Average density of the coolant, lb/in^3
V_{co}	=	Average coolant flow velocity, in/s
g	=	Mass conversion factor, equal to gravitational constant, 32.2×12 in/s^2
f	=	Friction loss coefficient
λ	=	Darcy-Weisbach friction coefficient
Re	=	Reynolds Number
k	=	roughness of duct

I. Introduction

Rockets have changed much from the earliest inception with China's creation of gunpowder to present day high-power liquid fueled engines. But modern high-power liquid engines have not changed much from the 1960's at all. The introduction of newer more efficient propellants spurred most of the change. As the means of propellants became more and more refined, the rocket itself needed to be improved with stronger, lighter, and more cost saving materials in order to be produced on a larger scale. The materials and tools to advance rocket engines since the 60's have not changed drastically and thus, modern rocket engines are not very different from the engines that were used to send the first humans to space and the moon. The two superpowers, being the USA and Russia, were pushing each other to create large and more powerful rockets to win the space race. American manufacturing methods were very precise, and thus most rocket engines developed were impinging designs for injector plates. Since Russian manufacturing methods, at the time, were not as precise as American manufacturing most liquid rocket they developed were based on pintel injectors. As the space race progressed it became more of a race for control and precision of manufacturing to reduce amount of defects while having the best performance. The race for higher performing, lighter weight, and more efficient engines were stymied by the manufacturing abilities of the time. Because of the inability to create certain passageways and geometries, the creativity of the engineers were restricted

[1] Undergraduate Student, Department of Mechanical and Aerospace Engineering, AIAA Student Member.
[2] Undergraduate Student, Department of Mechanical and Aerospace Engineering, AIAA Student Member.

to thinking in a conformed manner. Now, through additive manufacturing, we are able to unlock our imagination and think of completely innovative and novel designs for rocket engines.

Rocket engines are arguably one of the most complex devices in the field of engineering due to tolerances, material properties, temperatures, and pressures. Even though these marvels of engineering are difficult to manufacture correctly, there are a handful of companies developing and testing liquid engines. The market for engines is fairly niche, yet it is one with a significant amount of cash flow. Currently, the limitations for this technology deal with the production time, quality control, tolerances, and overall price per engine. There are a fair amount of competing products, yet not many engines specifically focus on production time or price but more on the quality and reusability.

As any liquid rocket engine comprises of two main systems, being the injector and the combustion chamber, taking advantage of additive manufacturing techniques enables the ability to reduce the systems to be 2 holistic components. The main advantages of utilizing additive manufacturing is decreasing the modes of failure, reducing production time, weight of the engine, and total manufacturing cost.

II. Background

The purpose of the injector is to take two propellants and uniformly distribute them over the area of the injector to atomize the propellants in order to ensure complete and stable combustion. The purpose of the combustion chamber is to convert the chemical energy from the propellants and convert them into kinetic energy. This works by first introducing fuel into the combustion chamber via the injector plate and then igniting the propellants, usually an oxidizer and a fuel for liquid rocket engines. Once the propellants ignite, the combustion chamber directs the chemical energy perpendicular to the injector in order to produce thrust.[2]

The challenge then becomes cooling the combustion chamber wall so that it does not melt due to the extreme temperatures produced by the combustion. Various cooling methods such as film cooling (when fuel is sprayed along the walls to create a boundary layer), regenerative cooling (when fuel is run along the walls of the engine to pull heat away from the material), or ablative cooling (when an insulated material is used to create a barrier between the combustion products and the wall) are used to keep the temperature of the walls well below the melting point of the rocket engine material.

Traditionally combustion chambers that took advantage of regenerative cooling were very difficult to make. The reason was that channels would need to be created in the walls. This was normally done by creating segments of the combustion chamber, then milling the channels in them, and finally welding all the pieces together. One could see how time consuming and complicating this process gets when an engine can have upwards of 100 channels running through the walls. Fortunately, additive manufacturing simplifies the process by creating one piece with very few post processing treatments.

III. Method of Creation

The manufacturing speed of the engine is a huge advantage of using additive processes over traditional machining. In what would normally take multiple weeks or even months to build, the engine took 160 hours to print continuously using a method known as Direct Metal Laser Sintering (DMLS). The engine was built on an EOS M270 which has an effective build chamber of 9.0x8.9x6.9 in.

The entire build took place in a nitrogen rich atmosphere. The engine, was built standing using the proprietary support system of the manufacturer, GPI Prototype Inc., to ensure that inner channels were created properly minimizing sag and burn. The post processing consisted of a laser weld of RP1 inlet tube, the pressure transducer port, a quick shot blast, and lathing the O-ring grooves. No other machining or heat treatment was done before it was shipped. Additionally, one of the great things about DMLS is that there is no waste in printing as you can sieve and reuse the powder unlike machining a part, with the metal chips and waste that occur.

To start the design process of the liquid engine, Rocket Propulsion Analysis (RPA), a software tool, was utilized to find the chamber geometry and as well as output combustion and propellant data. Below are the initial inputs and settings utilized to create such engine.

A. Initial Data

Engine Definition

- Chamber Pressure: 375 Psi
- Throat Diameter: 1.31 in

Propellant Specification

- O/F: 2.56

- Oxidizer: O2 (L)
- Fuel: RP-1

Nozzle Flow Model

Nozzle Conditions

- Contraction Area Ratio: 14.743
- Expansion Area Ratio: 5.93
- Frozen Equilibrium Flow enabled
- Freezing at the Area Ratio: 1

Nozzle Shape and Efficiencies

- Enabled Estimation of Efficiency of Nozzle
- Enabled Estimation for bell nozzle shape and efficiency for length 80% on basis of defined nozzle exit conditions
- Nozzle Flow Effects: (Enabled)
  - Consider multiphase flow and phase transition effects
  - Consider species ionization effects
  - Estimate performance loss due to flow separation in over expanded nozzle

Ambient Condition/Throttle Settings

- Ambient Pressure Range
  - 1->.37atm (.37atm = barometric pressure at 25000ft)
- Calculate estimated delivered performance

B. Performance and Thermodynamic Analysis

Refer to Appendix: *V1 RPA Chamber Performance Data*

C. Engine Design

Chamber Geometries

Design Parameters:

- Chamber Length: 6.25”
- Contraction angle b: 30 degrees
- R1/Rt: 1.49618
- R2/R2max: 0.500
- Rn/Rt: 0.382
- Parabolic approximation of the bell-shaped contour with fixed expansion area ratio Ae/At
  - Initial parabola angle Tn: 16.6 degrees
  - Final parabola angle Te: 14.94 degrees

D. Thrust and Mass Flow Rates with Chamber Geometry

Refer to Appendix: *V1 RPA Thrust Chamber Size and Geometry Data*

Injector Calculations:

Inputs

1. **Engine**
   - Chamber pressure; P_c = 375 Psi
   - Head loss coefficient (radius entrance); K = 1.2;
2. **Oxidizer**
   - Orifice Diameter; D_o = 0.0295 in
   - Mass flow rate; $\dot{m}_o$ = 2.0567 lb/s;
   - Density; ρ_0 = 71.5565 lb/ft^3 = 0.04141 lb/in^3;
3. **Fuel**
   - Orifice Diameter; D_f = 0.03 in
   - Mass flow rate; $\dot{m}_f$ = 0.8034 lb/s;
   - Density; ρ_f = 51.1488 lb/ft^3 = 0.0296 lb/in^3;

E. Injector Plate

First, a 20% pressure drop across the injector was utilized to ensure the resultant combustion products do not backtrack into the injector and potentially cause damages.

$$\Delta P = Pc * .20 \quad \text{psi}$$

The total injection area of both the oxidizer and fuel were separately calculated:

$$A_{total\ injection} = \dot{m}\sqrt{\frac{2.238K}{\rho \Delta P}} \qquad \text{in}^2$$

*ρ is in lb/ft^3

With the total injection area known and the diameter of each of the orifices known per oxidizer and fuel, the total number of orifices of each oxidizer and fuel can be determined.
First, the area of the orifice was calculated:

$$A_{orifice} = \Pi\left(\frac{D_{orifice}}{2}\right)^2 \qquad \text{in}^2$$

Then the number of orifices of fuel and the number of oxidizer orifices were found:

$$N = \frac{A_{total\ injection}}{A_{orifice}} \qquad \text{orifices}$$

N was rounded down to the nearest even number of orifices to maintain a minimum pressure drop and to have a set of complete like doublets.

In order to distribute the orifices throughout the face of the injector, the inner geometries (manifolds) were designed. It was decided that 2 oxidizer rings and 2 fuel rings were to be implemented. Based on the diameter of the injector plate, the manifolds needed to fit within that size envelope while still accounting for other engine designs such as the Trikes and film cooling. Thus, in order to determine the placement of the ring manifolds of the fuel and oxidizer, arbitrary radii where chosen in order to acquire an estimation of how many orifices would go on each ring. The designer, would then be able to resize the radii of those rings to optimize the geometry and performance while still maintaining the number of orifices per ring.

To find the number of orifices per ring, arbitrary radii were chosen, and then the circumference of each ring was calculated.

$$Circumference_{ring\ \#} = 2\Pi r \quad \text{in}$$

O Ring 1 r_1 = 0.5 in
F Ring 2 r_2 = 1.0 in
O Ring 3 r_3 = 1.5 in
F Ring 4 r_4 = 2.0 in

Next, the total circumference needed to be calculated for each the fuel and the oxidizer by summing rings 1 & 3 together and rings 2 & 4. Then the number of orifices per inch was calculated:

$$N_{per\ inch} = \frac{N}{Circumference_{total}} \qquad \text{orifices/in}$$

For each ring, we calculate the number of orifices per ring:

$$N_{ring\ \#} = N_{per\ inch}\ x\ Circumference_{ring\ \#} \qquad \text{orifices}$$

It was desirable to determine how acoustically stable the designs were so we the d/V ratio was found to see where it lied on the Hewitt plot. The bigger the orifices, the more acoustically stable the engine became but at the cost of fewer orifices and elements. Smaller holes are desirable for better atomization (mixing). In order to consider

stability, d/V >.00025 was set to act as stable after consulting with the Hewitt Plot as seen in **Figure 4**. Some stability compromises were made to achieve better atomization. Before finding the velocity, the mass flow rate coming out of an individual oxidizer orifice and an individual fuel orifice must first be calculated.

$$\dot{m}_{individual} = \frac{\dot{m}}{N} \qquad \text{lb/s}$$

Next, the velocities of the propellants coming out of the orifices were found:

$$V = \frac{144\dot{m}}{\rho A} \qquad \text{ft/s}$$

*ρ should be in lb/ft^3.

The ratio of D/V was determined to find its position on the Hewitt plot:

$$\text{d/V} = \frac{D_{orifice}}{V} \qquad \text{in/(ft/sec)}$$

If d/V is greater than .00025, we considered it relatively acoustically stable.

Moving on, it was desired to achieve similar momentums between the fuel and the oxidizer. Thus, the momentums were calculated:

$$M = V\dot{m}_{individual} \qquad \text{ft x lb/sec}^2$$

Once the injector was stable, according to the Hewitt plot, and matching momentums are achieved the manifold inlets were found using this rule of thumb: "Each manifold run 4x the flow area of the total group of injection orifices that are fed by it" (Huzel 107). From the Ignus injector design, the two fuel rings each have two inlets while the oxidizer rings are attached to the LOx Plenum and share one large inlet as seen in **Figure 1**. Thus, the fuel ring inlets were calculated:

Starting with Ring 4, the total injection area of this ring was found:

$$A_4 = A_{fuel\ orifice} N_4 \quad \text{in}^2$$

Multiply the total injection area by 4 according to the rule above. Since we have two inlets per fuel ring, we divided that value by 2.

$$A_{Inlet\ 4} = \frac{4A_4}{2} \quad \text{in}^2$$

Lastly, the diameter per inlet 4 was calculated:

$$D_{inlet4} = 2\sqrt{\frac{A_{Inlet\ 4}}{\pi}} \quad \text{in}$$

The above steps were repeated for fuel Ring 2 to calculate the diameter of the inlets of Ring 2.

Since the oxidizer rings share one large inlet, the diameter of that inlet was calculated as follows:

$$A_{oxidizer\ inlet} = 4\ x\ A_{Lox\ Total\ Injection} \qquad \text{in}^2$$

The diameters were then determined to be:

$$D_{oxidizer\ inlet} = 2\sqrt{\frac{A_{oxidizer\ inlet}}{\pi}} \qquad \text{in}$$

Here are the results:

FUEL Mass Flow Rate = .8034 lbm/s
OXIDIZER Mass Flow Rate = 2.0567 lbm/s

Diameter per oxidizer orifice = 0.0295 in
Total oxidizer injection Area = 0.046 in^2
Number of oxidizer holes: 66

Diameter per fuel orifice = 0.0300 in
Total fuel injection Area = 0.021 in^2
Number of fuel holes: 30

F Ring 4: Radius = 2.00 Perimeter = 12.57 # of Orifices = 20
O Ring 3: Radius = 1.50 Perimeter = 9.42 # of Orifices = 50
F Ring 2: Radius = 1.00 Perimeter = 6.28 # of Orifices = 10
O Ring 1: Radius = 0.50 Perimeter = 3.14 # of Orifices = 16

F # of orifices per inch: 1.592
O # of orifices per inch: 5.252

Fuel Velocity per orifice = 106.661 ft/s
Momentum = 2.856 ft x lb/sec^2
Fuel d/V = 0.00028 in/(ft/sec)
STABLE: since d/V > .00025 on Hewitt Plot

Oxidizer Velocity per orifice = 91.750 ft/s
Momentum = 2.859 ft x lb/sec^2
Oxidizer d/V = 0.00032 in/(ft/sec)
STABLE: since d/V > .00025 on Hewitt Plot

Inlets:
There are 2 inlets per fuel ring (x2 rings) and 1 large inlet to feed the oxidizer plenum!

Diameter per inlet of Fuel Ring 4 = 0.190 in
Diameter per inlet of Fuel Ring 2 = 0.134 in
Diameter of Oxidizer inlet = 0.484 in

F. Combustion Chamber

Inputting the above parameters, RPA is able to create an engine design profile as well as the mass flow rates of the oxidizer and fuel in order to reach the desired thrust. RPA is also then able to perform a chamber thermal analysis on the engine as well included cooling profiles such as regenerative cooling and film cooling. An initial constant rectangular channel for the regenerative cooling is used to find the maximum wall temperature. Then iterative steps are used to determine the optimal number of channels as well as channel geometries until the maximum wall temperature is below 1004 °F.

$$(1)\ 1/\lambda^{1/2} = -2\log[2.51/(Re\lambda^{1/2})+(k/d)/3.72]$$

$$(2)\ \Delta p=(f\, L\rho V_{co}^{2})/(2g)$$

A script was written in MATLAB to calculate the pressure drop throughout the combustion chamber using geometry data imported from RPA. The script utilized Colebrook's Friction Equation (1) and the pressure drop equation (2)[2], while assuming a straight flow in the calculations. Although minor loses were not calculated in the MATLAB program, the major loses were the quantity that was important because they would drive the design and optimization of the regenerative channels. A computational fluid dynamics program in SolidWorks was used to test different geometries for the collection chamber in order to minimize pressure drops. A straight perpendicular injection and a swirl injection was modeled and tested to see which would provide the smallest pressure drop.

Results from the MATLAB script were then used to alter the engine geometry in RPA and then the process was repeated in an iterative manner until an adequate cooling rate was achieved while minimizing the pressure drop

throughout the system. Once the system was optimized and finalized, the system was modeled using SolidWorks and a CFD analysis with Ansys was used to verify the validity of the pressure drop. The reason minimizing pressure drop is so important is that the rocket is using a pressure fed system. This means that the engine is limited to what pressures the tanks used can handle. For static fires, the large pressure drop is not a main concern because the large and heavy tanks could handle very high pressures. But for a flight ready system, the tanks needed to be light and could only withstand a certain pressure range. Finally using equations from Huzel, the wall temperature at the throat was calculated to verify the validity of RPA's thermal analysis.

IV. Design Constraint/Features

As with any manufacturing method, additive manufacturing has its limitations as well. Features that produce an overhang are unable to be printed without significant supports. Some supports are able to be incorporated with the design while others are not and need to be removed afterwards. It is important to minimize the need for supports that need to be removed because in some cases such as internal passages, supports won't be able to be removed. While outer elements can, the post processing drives up the cost of the part. With a supporting goal of minimizing the time and cost of manufacturing an engine, it is imperative that post processing is kept to a minimal by working with what the printer is readily capable of producing. However, advantages of additive manufacturing allows the ease of accurately printing designs that traditional manufacturing methods are unable to reproduce.

A. Injector Plate

The impinging injector was modeled to follow the iconic F-1 rocket engine with alternating fuel and oxidizer rings that utilized like-doublets to independently spray each propellant.[1] The flow in each ring was directionalized to create a constant and laminar flow and reduce turbulence in order to decrease the amount of energy lost. With the ability to create geometries that were seen as impossible with traditional manufacturing, this injector utilizes dynamic pressures rather than static pressures which allow us to reduce ring and propellant collection chambers sizes. By utilizing dynamic pressures, the manifolds are created to continuously and fluidly distribute the propellants with the least amount of abrupt stops and starts.

In addition to a unique propellant distribution manifold, the downcomers from each ring were created to flow with the directionalization of the ring and follow the path until the propellants can be redirected into a like-on-like configuration.[2]

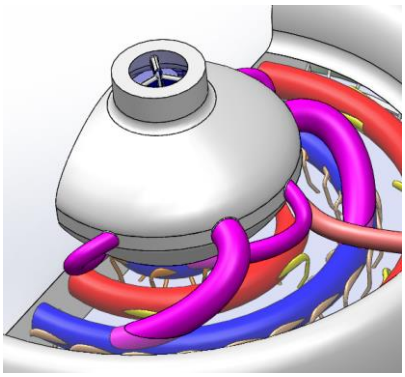

Figure 1. *Propellant Manifolding.*

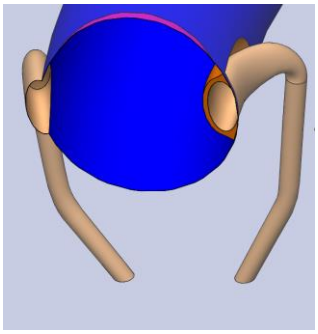

Figure 2. *Outer downcomer (left) inner downcomer (right).*

The like doublets were designed to extend the combustion chamber life and reduce the amount of oxidizer that would contact the walls.[2] Since each of the rings are directionalized, there will be propellant flowing in the rings which will create a centrifugal force pushing our propellants towards the outer edge of ring. The goal of the downcomers is to have a defined cross sectional area that is perpendicular to the flow.[2] With the centrifugal force it is easy to design a downcomer that will follow the tangent line of the ring so that the propellant will flow into it. The inner downcomer would be negatively affected by the centrifugal force and thus is designed to protrude into the ring in order to obtain the desired cross sectional area that is perpendicular to the flow.

Having four propellant rings allowed for the outermost rings to be fuel and alternated with the oxidizer until the innermost rings (**Figure 3**).

Ring 4, the outermost ring, was chosen to be fuel to act as a film cooling barrier and the resultant impingement angle was canted towards the center of the throat to funnel the other propellants away from the walls of the combustion chamber. The impingement of the inner most ring, Ring 1, was canted towards the next outer ring, Ring 2, in order to create more uniform propellant mixing. Rings 2 and 3 have impingement resultants that are perpendicular to the injector face.[2] Through an iterative process, the number of fuel orifices and velocities of each element were calculated to be stable on the Hewitt Plot.

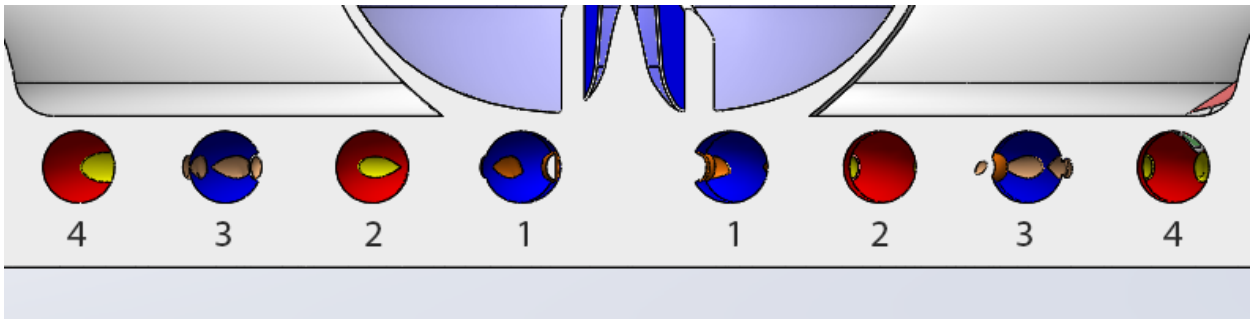

Figure 3. Propellant Rings. *Cross section of the propellant rings. Blue rings represent oxidizers while red represents fuel.*

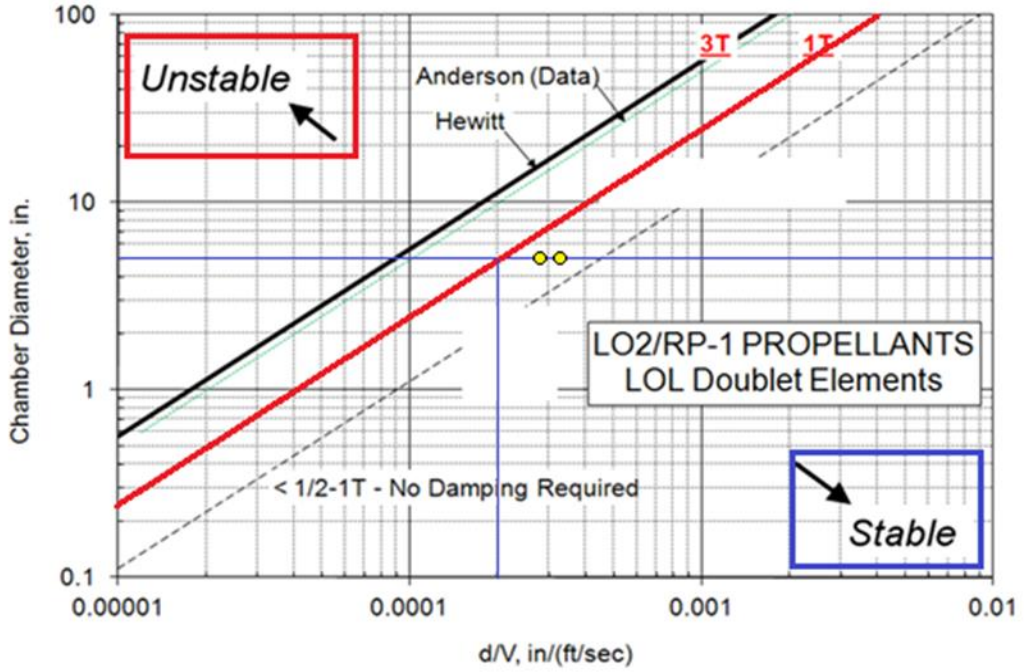

Figure 4. Hewitt Plot. *The Hewitt Plot uses experimental data to create a correlation with chamber diameter and exit velocity in order to determine possible instabilities. Have a chamber diameter of 5" with a goal of being on the bottom right hand side of the 1T line (Red), an iterative process was taken to account for minimum printable orifice size and exit velocity of each individual propellant. Both propellants are shown to be on the bottom right area of the graph, as seen with light blue circles on the dark blue line towards the center of the graph.*[4]

In order to ensure that each ring has an even distribution of propellants collection chambers were created for both the oxidizer and the fuel. The collection chambers allow for an equal static pressure to build up in order to evenly distribute the propellants to the rings through 'arms'.

Having a regeneratively cooled engine, the collection chamber for the fuel is in an annular form and acts as a larger outer ring to distribute the fuel to the inner rings. The oxidizer collection chamber is quite different in that the inlet for the oxidizer is in the center of the injector but still created a static pressure to evenly distribute the propellants in the directionalized rings. To help promote laminar flow in the oxidizer manifold, a feature was created to smoothly distribute the incoming propellant by utilizing a conical shape to redirect the propellants around it into the manifold.

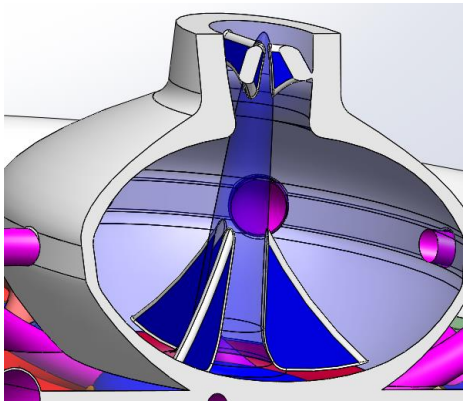

Figure 5. Splash Cone.

The injector on a whole was designed to slash weight and is visually seen with the exterior pipes leaving the oxidizer manifold and the pipes from the regenerative cooling collection chamber to the independent fuel rings. This injector was designed to be a research and development prototype, which allowed for instrumentation ports to be integrated in the part. NPT fittings were added to the

injector to allow for pressure transducers to physically be mated. In addition to adding the fittings, a .030" diameter service line over 8 inches in length was created from each ring to the transducer ports to both allow for pressure readings and create a cushion of air between the propellants or hot gases and the transducers. In order to create a lengthy service line in such a compact space, helical tubes were created and then connected in series with the pressure transducer and the feature of interest.

Having the ability to integrate instrument ports and such features decreases chances for plumbing errors and overall weight while increasing longevity of the instruments and also having the ability the fly the injector without instruments. Learning from the first engine that was printed by SEDS UCSD, the injector was not welded on to the combustion chamber to allow for reusability and inspection of both the injector and combustion chamber pre and post hot fire tests. In order to mate both components, O-rings were utilized to seal the fuel and connect the system together. The O-ring grooves were designed into the injector face while the combustion chamber mating surface was flat. The grooves were designed into the injector face, and not the combustion chamber, because post processing is required to make the features have a low enough surface roughness for the O-rings to properly seal.[3] Machining the O-ring grooves isn't an entirely difficult process, but to remove any chances for damage to occur to the engine, the injector was chosen because of its compact size and overall robustness, if placed on a lathe. An important factor that was necessary to consider when designing this injector, to be additively manufactured, was a problem with the particulate size and the laser resolution resulting in smaller orifices than designed for. To account for the shrink factor present in all additively manufactured components, coupons were printed of various sizes and geometries and then analyzed with a laser measuring tool to send back the printed dimensions and account for the error.

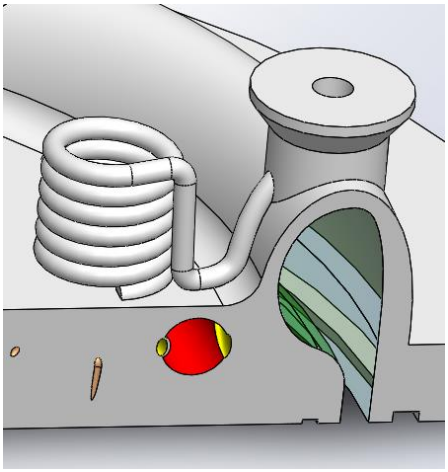

Figure 6. Helical coil *for pressure transducers***.**

B. Combustion Chamber

One of the unique features additive manufacturing allows is creating regenerative channels that could be complex in design but easily printed. The regenerative channels were initially designed to be rectangular, but were later changed to have the side closest to the chamber walls follow the contour of the chamber walls (to promote more surface area) as well as the wall furthest from the wall to be a semicircle (to reduce pressure drop) seen in **Figure 9** . Another feature that was considered, but not implemented was a spiral regenerative channel. In theory the design would better cool the engine; however, the DMLS printer being used is not able to reliably print that design due to concerns of warping propagation. A vital design component was the addition of the trikes to help stabilize the engine. The trikes are 3 protrusions that extend down the walls of the combustion chamber that are used to increase the frequency of the tangential instabilities. This is necessary because the lower frequency tangential instabilities can cause the engine to fail and tear apart. This protrusion is a cause for concern because it extends further into the engine so the regenerative channels also had to be moved in to be close to the wall to maintain adequate heat transfers. One of the challenges posed with additive manufacturing is the geometries that can be printed in certain directions. For instance, the fuel inlet leading into the collection chamber at the bottom of the combustion chamber has a splitter that requires a larger opening. With the direction the engine is being printed, support structures need to be printed in order to accommodate the design. Being an internal passage, normal support structures could not be used because it would end up blocking the passage so arches were used to support that open structure to prevent print failure. To also prevent warping, the inlet pipe will be printed separately and welded on afterwards. Another challenge of additive manufacturing is the shrink factor involved with the print jobs. Every material has a different shrink factor so it was found that a coupon was needed to test for the shrink factor to account for critical geometries to ensure accuracy. Once the shrink factor is found, the model is then adjusted to account for the shrink factor.

V. Test Configuration

The engine was tested in the Mojave at the Friends of Amateur Rocketry site using a static fire system built by UCSD SEDS. The main purpose of this first engine is to test how closely the calculated values match the actual values. Most notable is the cooling of the engine because this first design incorporates extra film cooling to ensure adequate cooling. Once the data comes back, the film cooling can be reduced to create a more optimal design. The

data that the static fire system will be collecting include pressure readings from various passages in the engine, temperature readings of the fuel as well as the engine, the thrust levels, and the osscilations of the engine.

Pressure transducers were placed in the Combustion Chamber Inlet Plenum, the RP-1 Injector Plenum, in each propellant ring, and the combustion chamber through the injector face reading measurements at a frequency of 5 KHz. The purpose of having the pressure transduces in both collection chambers is to calculate the overall pressure drop through the regenerative channels to verify the calculations along with the CFD analysis. This also helped to calibrate the pressurization of the propellant tanks. The pressure transducers in the propellant rings were intended to verify if the dynamic pressure design incorporated acts as predicted. The pressure transducers in the combustion chamber were intended to verify if the calculated pressure and the actual pressure were measured as expected in order to verify the total thrust output and pressure drop across the injector plate.

Thermocouples were used to record the temperature of the exterior surface of the combustion chamber and the injector plate. A load sensor measured the thrust output of the engine. This was mounted on a linear bearing slide to reduce friction to allow for an accurate measurement of the thrust and the longitudinal instabilities. The data gathered here will provide better insight on how to better design the next injector plate to produce a more efficient design.

The system was designed to be a pressure-fed system, thus allowing for constant thrust and pressure measurements throughout the combustion chamber and injector plate. Unfortunately, flow restriction problems with the dome regulator of the pressurizing system inhibited the static fire system from being truly pressure-fed and thus was partially a blow-down system.

VI. Theoretical Results

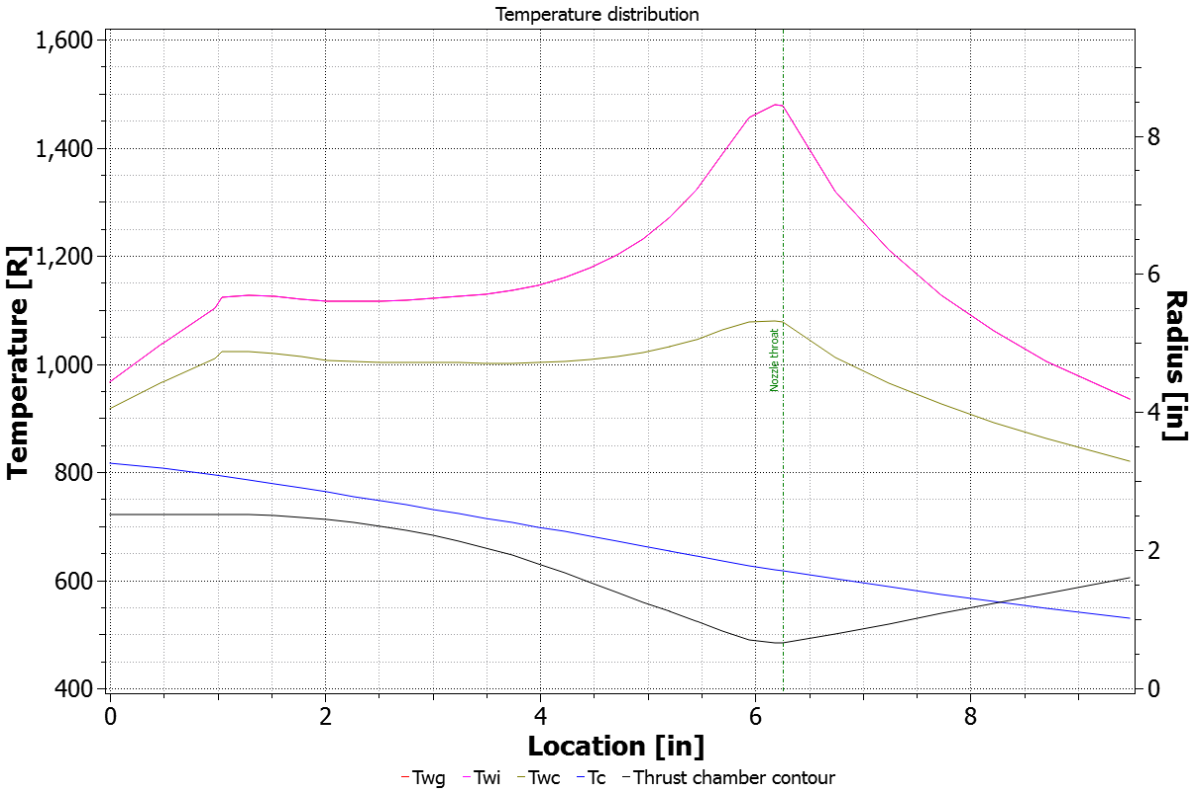

Figure 7. Temperature distribution of a constant rectangular channel. *This created a pressure drop of 467 psi.*

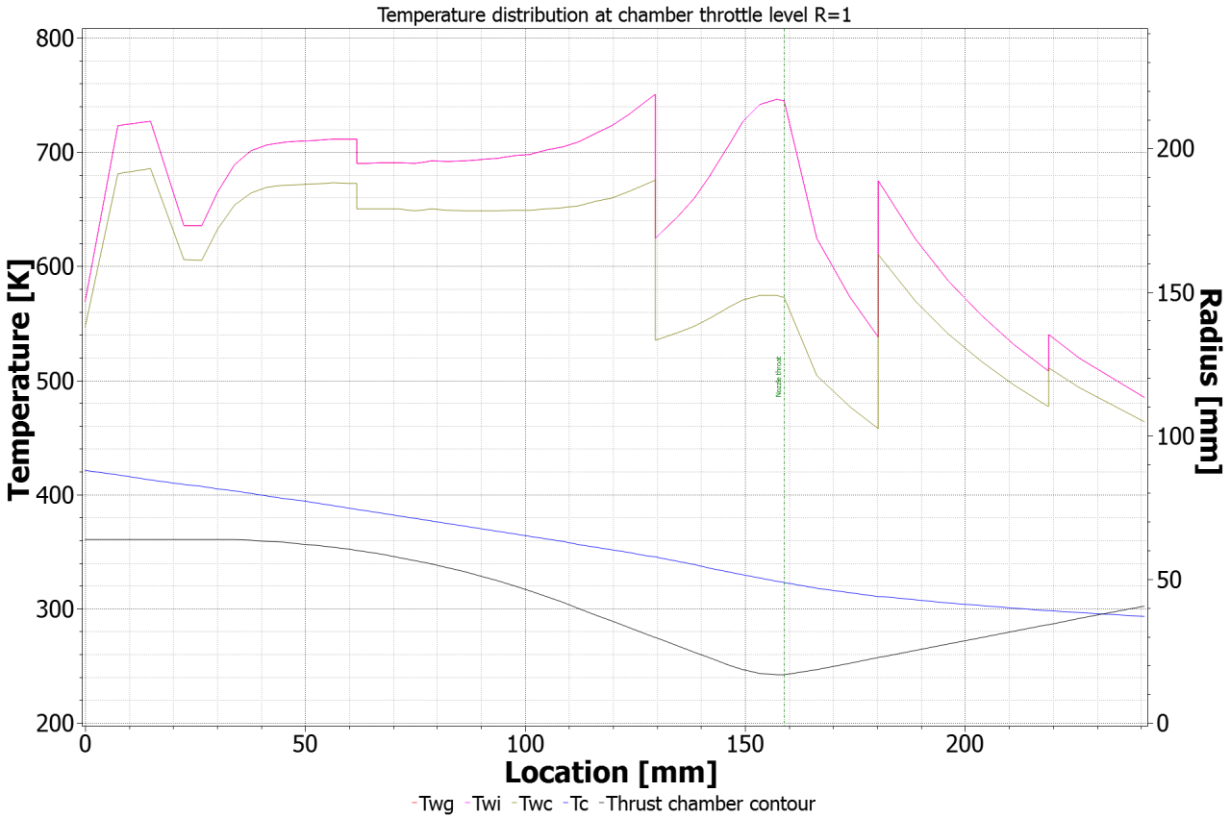

Figure 8. Temperature distribution of a varying rectangular channel. *This created a pressure drop of 105 psi.*

With a constant regenerative channel with film cooling yielded this result in **Figure 7**. However this caused the pressure drop to be very large. To minimize the pressure drop, the channels were varied so that the temperature gradient would be more constant and this allowed for larger channels, which in turn minimizes the pressure drop (**Figure 8**). To minimize the pressure drop, the channels were changed from a rectangular shape to the shape discussed in the Design Constraints/Features section an also shown in **Figure 9**. This allowed the pressure drop to be reduced down to 85 psi. This means that the design allowed for a 20% reduction in pressure drop by choosing a more optimal shape.

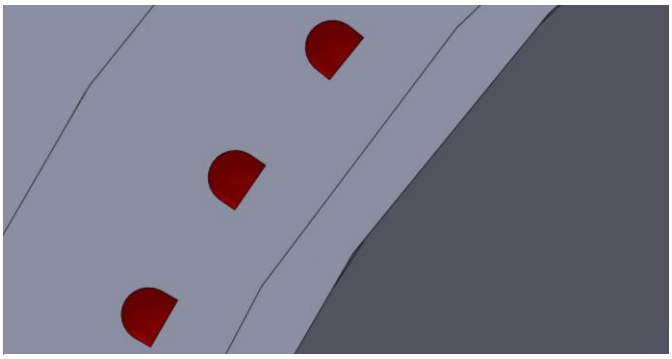

Figure 9. Regenerative Channel Cross Section Design *This design helps optimize heat transfer and minimize pressure drop.*

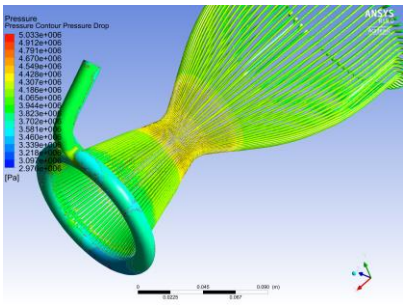

Figure 10. Ansys CFD Analysis

To further analyze the pressure drop, a CFD analysis using Ansys was done to verify the outcome in **Figure 10**. The exit pressure was defined as 500 psi and it was found that the inlet pressure would be 589 psi. This meant that there would be an overall pressure drop of 89 psi. The numbers from this CFD study support the equations used to derive the pressure drop.

Reexamining **Figure 8**, the temperature is kept below 1000 °F because Huzel noted that wall temperatures below 1000 °F were considered effectively cooled[1]. This was met with some room for error by increasing the film cooling to be 20% of the total mass flow rate. As stated before, this engine is not optimized, but is a safe starting point for the next injector designs to be optimized. The film cooling was needed because the material Inconel 718 did not have a high enough thermal conductivity. Most small engines that are exclusively regeneratively

cooled use copper because it has a thermal conductivity greater than 14.4 BTUin/(hin^2°F). Inconel 718 has approximately a thermal conductivity of .96 BTUin/(hin^2°F). This large difference meant that the walls needed help to be cooled, which is where the film cooling was found to be necessary. Copper was not used before because it was not readily available to be printed so the material itself became a constraint that drove the design of the engine.

VII. Experiment Results

The culmination of multiple hot fires and cold flows resulted in the experimental data obtained. A hot fire is defined as a combustion process occurring from burning propellants in a controlled matter to produce thrust at specified tank pressures. A cold flow is defined as a test of the system at the correct pressures but with inert chemicals instead of reactive propellants. Liquid Nitrogen was used instead of Liquid Oxygen and water was used instead of RP-1 for substitutes of the reactive propellants during the cold flow. The purpose of a cold flow is to test the system at cryogenic temperatures and to ensure that all operations are practiced and understood with inert chemicals rather than reactive substances. A total of three hot fires and numerous cold flows were conducted, but data was obtained from only the last two hot fires and one cold flow operation.

Figure 11 is included to indicate the specific features that are being measured with pressure transducers while **Figure 12** is added to detail the location of the thermocouples on the engine. Below is a summary of the pressures and temperatures recorded from the operations.

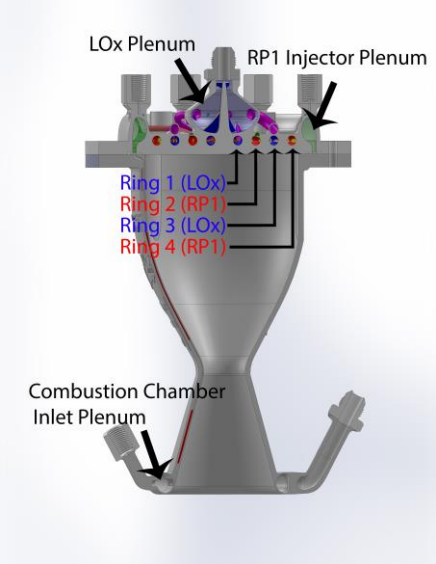

Figure 11. Engine Pressure Transducer Legend

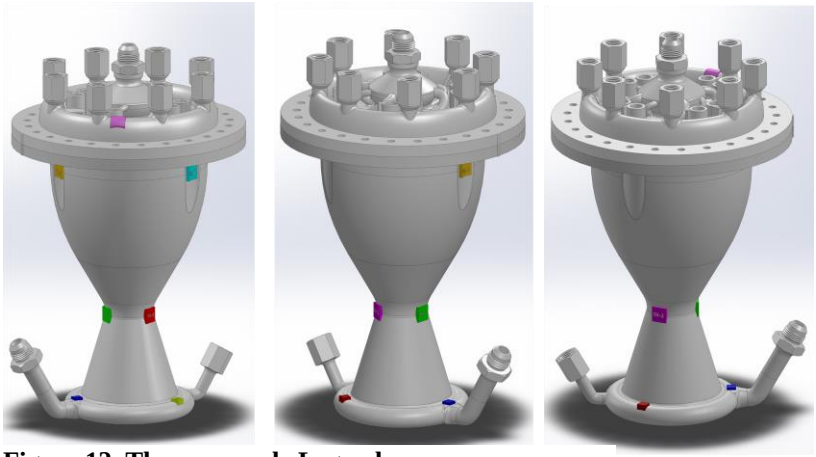

- *RP-1 Injector Plenum [■]*
- *Trikes 1&2 120° away from each other[■ ,■]*
- *Throat 1&2&3 120° away from each other[■,■,■]*
- *Inlet Plenum 1&2&3 120° away from each other[■,■,■]*

Notes: All Throat and Inlet Plenum Thermocouples are vertically under a Trike

Figure 12. Thermocouple Legend

Title	Cold Flow		**Flow Time [sec]**	3.2

LOx PT's [psi]	*Start CF*	*End CF*	*Range*	*Average*
Tank	744.5	647.2	647.2-744.5	692.6
Plenum	573.0	560.2	493.9-573.8	526.7
Ring 1	541.4	545.3	473.4-555.9	501.6
Ring 3	546.3	546.6	481.2-558.7	507.9

RP-1 PT's [psi]	*Start CF*	*End CF*	*Range*	*Average*
Tank	779.7	705.3	705.3-779.7	729.4
CC IP	751.0	683.0	682.6-753.0	707.0
Injector Plenum	678.6	765.9	658.2-767.1	702.6
Ring 2	665.0	749.1	649.7-750.2	691.7
Ring 4	16.9	16.8	8.6-18.9	13.6

Other PT's [psi]	*Start CF*	*End CF*	*Range*	*Average*
Injector Face 1	16.5	16.4	10.5-18.3	14.4

TC's [°C]	*Start CF*	*End CF*	*Range*	*Average*
Trike 1	-23.7	36.1	-24.0-36.1	16.3
Trike 2	-16.2	31.2	-17.0-31.2	14.0
Injector Plenum	17.8	33.3	17.3-33.3	24.2
Throat 1	-37.9	39.0	-39.1-39.0	18.9
Throat 2	-19.2	39.6	-20.0-39.6	23.8
Throat 3	-30.0	41.6	-30.4-41.6	28.0
CC IP 1	34.8	44.5	34.5-44.6	42.8
CC IP 2	22.6	43.8	22.4-43.7	39.4
CC IP 3	21.8	43.8	22.4-43.8	39.4

	Start HF	*End HF*	*Range*	*Average*
Thrust [lbf]	30.8	29.8	24.5-42.9	32.1

Injector Face 2	12.9	13.5	5.45-14.5	9.9

Chart 1. Data from Cold Flow

Title	Hot Fire 2	**Burn Time [sec]**	1.69

LOx PT's [psi]	*Start HF*	*End HF*	*Range*	*Average*
Tank	401.7	375.3	375.3-401.7	389.7
Plenum	135.4	224.3	135.4-256.1	210.9
Ring 1	293.1	291.5	260.3-302.2	285.8
Ring 3	10.7	31.1	10.7-31.1	20.6

RP-1 PT's [psi]	*Start HF*	*End HF*	*Range*	*Average*
Tank	437.8	408.1	408.1-437.8	421.0
CC IP	122.7	395.3	122.7-409.1	343.8
Injector Plenum	69.1	368.5	69.1-383.5	300.9
Ring 4	55.4	337.8	55.4-350.6	262.7
Ring 2	.4	.5	.2-2.5	1.2

Other PT's [psi]	*Start HF*	*End HF*	*Range*	*Average*
Injector Face 1	.2	20.2	.2-20.2	11.1
Injector Face 2	-1.5	.8	-1.5-.8	-.7

TC's [°C]	*Start HF*	*End HF*	*Range*	*Average*
Trike 1	N/A	N/A	N/A	N/A
Trike 2	N/A	N/A	N/A	N/A
Injector Plenum	N/A	N/A	N/A	N/A
Throat 1	N/A	N/A	N/A	N/A
Throat 2	N/A	N/A	N/A	N/A
Throat 3	N/A	N/A	N/A	N/A
CC IP 1	N/A	N/A	N/A	N/A
CC IP 2	N/A	N/A	N/A	N/A
CC IP 3	N/A	N/A	N/A	N/A

	Start HF	*End HF*	*Range*	*Average*
Thrust [lbf]	419	292.1	240-418	291.9

Chart 2. Data from Hot Fire 2

Title	Hot Fire 3 **Hard Start**	**Burn Time [sec]**	.67

LOx PT's [psi]	*Start HS*	*End HS*	*Range*	*Average*
Tank	689	705.1	689-706.7	702.6
Plenum	609.2	651.7	608-651.7	633.2
Ring 1	585.2	638.6	585.2-639.5	623.1
Ring 3	570.8	638.4	570.8-656	629

RP-1 PT's [psi]	*Start HS*	*End HS*	*Range*	*Average*
Tank	846.9	759.3	759.3-846.9	789.8
CC IP	45.0	944.9	44.9-945.1	547.7
Injector Plenum	47.4	665.6	40.2-679.3	258.6
Ring 4	27.2	666.5	20.6-706.2	252.5
Ring 2	14.9	15.5	6.7-18.0	12.8

Other PT's [psi]	*Start HS*	*End HS*	*Range*	*Average*
Injector Face 1	21.4	21.0	10.3-75.6	20.4
Injector Face 2	17.4	14.0	5.6-71	13.4

TC's [°C]	*Start HS*	*End HS*	*Range*	*Average*
Trike 1	N/A	N/A	N/A	N/A
Trike 2	N/A	N/A	N/A	N/A
Injector Plenum	N/A	N/A	N/A	N/A
Throat 1	N/A	N/A	N/A	N/A
Throat 2	N/A	N/A	N/A	N/A
Throat 3	N/A	N/A	N/A	N/A
CC IP 1	N/A	N/A	N/A	N/A
CC IP 2	N/A	N/A	N/A	N/A
CC IP 3	N/A	N/A	N/A	N/A

	Start HS	*End HS*	*Range*	*Average*
Thrust [lbf]	827.9	991.3	762-1090.4	903.6

Chart 3. Hard Start Data from Hot Fire 3. *TC's could not accurately read temperatures in such a short time frame during the Hard Start so were omitted from results.*

Title	Hot Fire 3 **Normal Combustion**	**Burn Time [sec]**	3.35

LOx PT's [psi]	*Start HF*	*End HF*	*Range*	*Average*
Tank	705.1	686.8	686.8-705.1	691.5
Plenum	651.7	619.2	585.4-651.7	597.7
Ring 1	638.6	605.6	575.4-639.6	584.1
Ring 3	638.4	607.4	579.6-641	586.8

RP-1 PT's [psi]	*Start HF*	*End HF*	*Range*	*Average*
Tank	759.3	751.4	751.4-763.6	757.8
CC IP	944.9	736.3	664.1-944.9	740
Injector Plenum	665.6	732.3	649.4-735	703.1
Ring 2	666.5	745.6	646.8-749.1	704.8
Ring 4	15.5	14.0	7.8-29.1	13.3

Other PT's [psi]	*Start HF*	*End HF*	*Range*	*Average*
Injector Face 1	21.1	18.4	13.9-36.9	18.1
Injector Face 2	14.0	11.8	6.3-29.3	11.4

TC's [°C]	*Start HF*	*End HF*	*Range*	*Average*
Trike 1	-33.5	42.2	-34-102.4	51.2
Trike 2	-37.7	40.6	-38.4-61.7	33.1
Injector Plenum	11.5	41.5	11.3-49.9	38.4
Throat 1	-36.5	38.3	-36.9-79.1	39.5
Throat 2	-24.8	39.7	-25-47.5	31.8
Throat 3	-33.1	40.8	-33.4-102.2	46.2
CC IP 1	30.9	44.7	30.7-48.4	43.4
CC IP 2	22.1	43	21.8-50.2	41.7
CC IP 3	10.6	37.6	10.6-51.4	38.8

	Start HF	*End HF*	*Range*	*Average*
Thrust [lbf]	991.3	649.2	614.5-991.3	644.7

Chart 4. Normal Combustion Data from Hot Fire 3

PT's=Pressure Transducers

TC's= Thermocouples
CC IP= Combustion Chamber Inlet Plenum

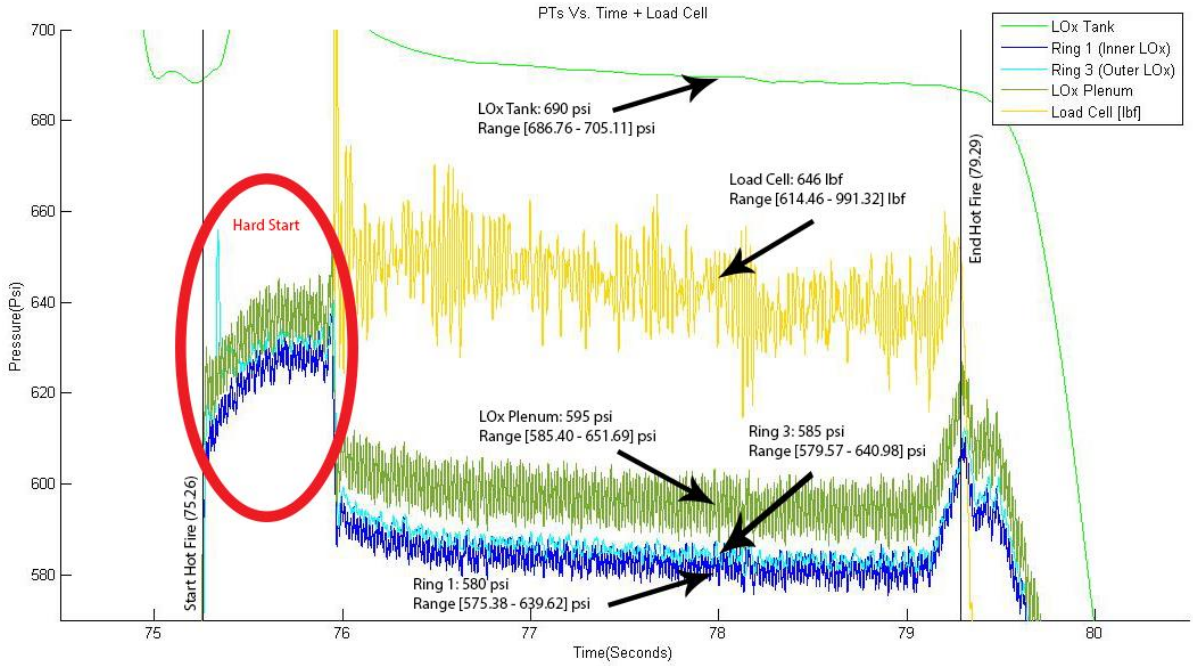

Figure 13. Hot Fire 3 Normal Combustion LOx Data

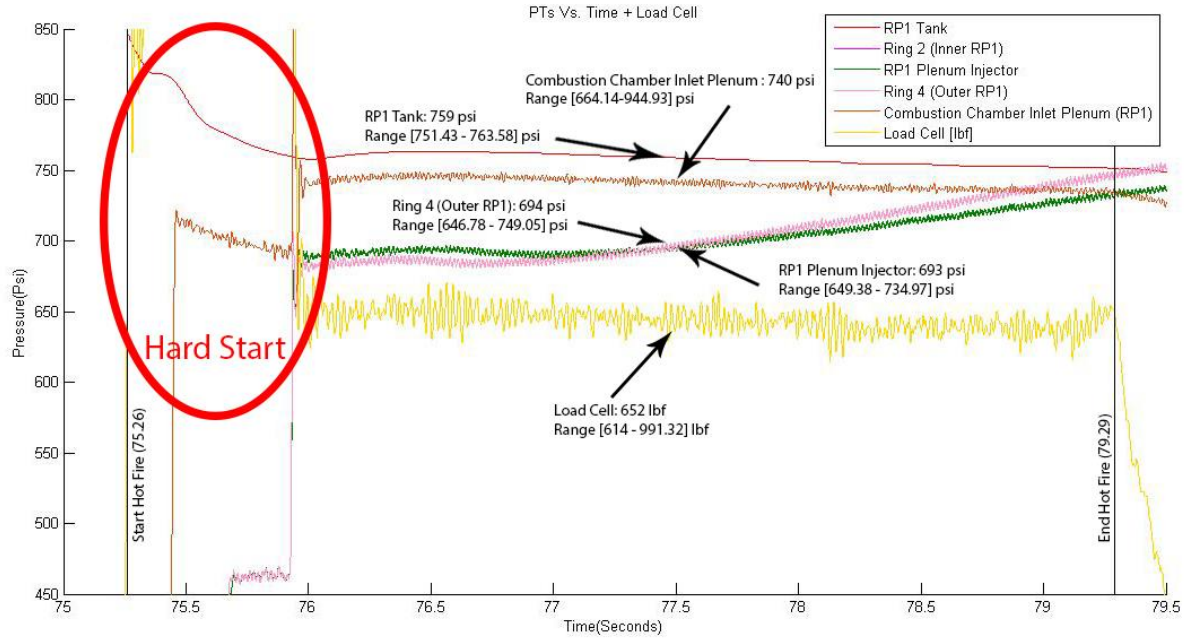

Figure 14. Hot Fire 3 Normal Combustion RP-1 Data

Thermocouples were not integrated on the engine during the testing of Hot Fire 2 which is why temperature data is not available. Because the thermocouples are dependent on the surface of the feature to increase in heat before data is obtained, temperature data is not available for the Hard Start portion of Hot Fire 3. There was not enough time for the surface of the engine to increase in temperature which is what resulted with no measured change in temperature during those specific times of the Hot Fire. All of the temperature data in **Chart 1** and **Chart 4** is

visually shifted in time from the actual occurrence of the event to match when the thermocouples actually measured the data. This is done to account for the time it takes for heat to be conducted through the surface of the combustion chamber.

VIII. Discussion

During the testing of this engine, a total of three hot fires and one hard start occurred. The system and engine went through more than 5 cold flow tests in order to ensure functionality and that all personnel understood roles. This engine has a total burn time of 6.66 seconds and has reached a stable and sustained maximum thrust of 645 lbf. Having the ability to vary pressure in the tanks allows for accountability of pressure drops in the system and the engine, thus ensuring proper flow rates through the injector. The goal from testing was to determine the pressure drops across the LOx Plenum, RP-1 Plenum, and the regenerative cooling so that the system can be recalibrated to ensure proper mass flow rates from each propellant is exiting the injector. Once confirmed that the pressure in each of the propellant rings are equal, it can be assumed that the desired mass flow rate is obtained through the injector. Results from the cold flow tests were utilized to determine pressure drops and head losses as follows. There is a noticeable pressure drop of 30 psi across the static fire system measured at the Combustion Chamber Inlet Plenum. Unexpectedly, a pressure drop across the regenerative cooling of 74 psi was measured versus the theorized 89 psi contributed due to an estimated surface roughness as well as change in area. A minimal loss of 13 psi is seen from the injector plenum to Ring 4 resulting in an overall pressure drop averaging at 110 psi from the RP1 tank to the propellant ring in the injector. Though Ring 2 did not receive proper data, it can be assumed that the ring was flowing freely as tests were successfully conducted before the hot fire to inspect impingement and powder blockage. The head loss noticed from the LOx plenum to the rings resulted in a value of 20 psi. Though a minimal head loss was measured from the LOx plenum to the rings, a large pressure drop was seen across the system from the Propellant feed tank into the LOx plenum itself of 170 psi resulting in an overall pressure drop averaging in 190 psi for the system to a propellant ring. Given that this injector was designed to utilize dynamic pressure rather than static pressure in the manifolds, a measurement anomaly was the only noticeable problem present during testing.

Anomalies occurred during the measurements of Ring 4 and the Injector Plenum as seen in **Appendix C: Figures 1 and 3** when the pressures were seen to rise throughout the hot fire as well as the cold flow. Pressure data obtained from Ring 4 and the Injector Plenum are shown to have a pressure higher than the stagnation pressure, which is defined by the propellant tank pressure. Subsequent to an abnormally high pressure in both injector locations, lengthy oscillations were produced that diminished the pressures to follow the tank pressures more closely. Oscillations lower than .33 Hz were present in the measurements, which are not ordinary to see in these experiments. It is extremely odd to have these measurements occur in both the cold flow and hot fire 3. Hot fire 1 and 2 utilized a different data acquisition system, which may have prevented this anomaly from occurring. The oscillations appear to originate from Ring 4 and propagate to the Injector Plenum because the peaks and sharp drops are mirrored very closely in the plenum from what is measured in Ring 4. This is not due to a combustion instability because the measurements were seen in both the cold flow and the hot fire. Thus, it is believed that this anomaly is occurring due to an artifact of our measurement methods. As this system was designed to utilize dynamic pressures rather than static pressures, an anomaly was seen to have occurred during the measurement of a fast moving fluid with a static pressure reading transducer.

The hard start of the engine lasted a total of .67 seconds and averaged 904 lbf while peaking at 1090 lbf for an instant at ignition. Unfortunately the pressure transducers were unable to give us a reading of the chamber pressure. But using RPA, it showed that a 900 lbf correlates to a chamber pressure of over 450 psi. Looking at the worst case scenario, thin wall assumption, the hoop stress is 9825 psi at room temperature. The yield strength of the material in the xy direction is 113 ksi at room temperature. This means there is a safety factor of 10 without accounting for thermal stresses. Note that this calculation for hoop stress does not include the effects of the channels and the pressures within them. The hard start can be partially attributed to the detonation of residual Jet-A fuel stagnant in the combustion chamber after two initial failed firing attempts. During the hard start, LOx and Jet-A are atomizing but only igniting outside the throat. Due to the limited resources, the combustion chamber was never hydro-tested before the test fires. But after the third hot fire, which was a hard start, gouges in the throat appeared and it became apparent that a hydro-test was needed to check for cracks. An aluminum plate with O-ring grooves was fashioned to allow the combustion chamber to be hydro-tested using a pressure washer. The combustion chamber was hydro-tested to 400 psi. It was then apparent that three pin holes were found in the same section the gouge was. Although three separate streams were found in the same section, this could mean that rather than 3 different holes, this could be one crack. At the moment, options are being weighed on how to fix the crack. Another important aspect of the hydro-test was that it showed two pinhole leaks on the fuel inlet weld. This was most likely always present and not a

result of the hard start. But not long after this was discovered, one of the members was fitting the engine to the rocket and forgot to counter torque the fuel inlet. This caused the fuel inlet to crack open along the pin holes. Structurally the weld was the weakest point and the pin holes meant the section was not properly welded, further weakening the section. The part was fixed by rewelding the section.

It is important to note that even if the reason the crack occurred during the hot fire was not because of the hard start, it may be due to the prolonged burn time. The previous two times were burp tests with only 1.5 seconds of burn. The third test was about 4 seconds, more than twice the duration. The duration may have played a large role because it allowed the material to be heated up further than the previous tests. From the hot fire data, it seems to show that none of the thermocouples used ever reached a steady state. This implies that if the test had been longer, the engine may have been able to heat up even further. Another reason could be that the engine was designed to use RP-1 as its fuel, but every hot fire used Jet-A. The differences in fuel may have caused some compatibility issues but are very unlikely because both are derivatives of kerosene and both have comparable thermal properties such as specific heats and thermal conductivities. Another issue could be orifice/channel geometries. They were not thoroughly checked and could have caused inadequate impingement or cooling. Inspecting the impingement of the LOx passages shows multiple jets missing impingements which could cause an almost 180 degree burn on both sides of the combustion chamber. If a jet misses impingement to its partner orifice, it can cause a hot spot on the direct opposite side of the combustion chamber or throat which they are combusting in. While conducting flow tests of the injector, multiple LOx orifices are seen to misimpinge creating LOx streams that do not atomize but still interact with the throat of the engine. This possible interaction of high temperature LOx streams with the throat of the combustion chamber can attribute to a large reason why this crack occurred. Not having a constant velocity duct for the collection chamber for the combustion chamber could have caused inadequate flow and inadequate cooling; however, this is unlikely because the side with the least flow was not the side that was damaged.

Another important shortcoming of DMLS is the shrink factor. Depending on the software the 3D printer uses, shrink factor can change. In our case, the printer sinters the inner most radius of the circle and in doing so, it may sinter slightly more than intended due to powder resolution. On larger scales, the effect is not as important or noticeable. But when printing orifices that are 0.030”, the relatively small differences are no longer relatively small and could possibly close up the hole. With limited time, information, and resources, we added 0.005” to all orifice diameters to hopefully account for some of the shrinking. We did not have the capabilities to measure if the orifices came out to the correct orifice sizes and that may have affected the injection area needed. This in turn affects the performance of the engine as well as the thermal properties needed. Also not having the correct orifice sizes throughout the combustion chamber affects the pressure drop through the system. It is believed that our compensation with orifice area shrinkage may have been too low since we are not obtaining the desired thrust which is very closely related to chamber pressure. If injection area is smaller than expected, it can cause a higher pressure drop resulting in a lower combustion chamber pressure. Examining the propellant rings to be 500-600 psi, a 20% pressure drop should result in a chamber pressure of 400-480 psi. Unable to measure combustion chamber pressure, due to irremovable powder in the service line, it can be inferred that the desired combustion chamber pressure is not being met thus not resulting in the thrust designed for. In addition to the shrinkage in injection area, the presence of multiple blocked orifices in the injector of both propellants can account for a high pressure drops across the injector and low thrust. It is important to note that all of the AN and NPT fittings were printed and did not have to be retapped or chased with a die.

IX. Conclusion

The designing, printing, and successful testing of a fully additively manufactured liquid engine is a testament that the technology has the potential to redefine how engines are designed and manufactured in the future. Data obtained from hot fires and cold flows do show considerable head loss of 110 Psi and 170 Psi, in the RP-1 and LOx manifolding respectively, caused by a relatively high surface roughness. As DMLS technology becomes more refined and layer resolution is developed to be more precise, surface roughness and material variabilities will decrease and create smoother more homogeneous products. With a total burn time of only 6.66 seconds, this engine is not yet close to being certified for hardware flights but is a large step in utilizing additive manufacturing to develop new designs that have the potential to revolutionize how rocket engines are created. The creation of an impinging injector that utilizes dynamic pressure rather than static pressure tackled quite a few problems at once and hopefully will be a pathway for a new line of research that can change how injectors are perceived. The ability for this engine to be completely additively manufactured and tested successfully on its first try is a feat that can hopefully be replicated by many individuals to show the ability this technology has to rapidly change this field. With a maximum sustained and stable thrust of 645 lbf, the engine has the power to launch a small sounding rocket and be a proof of concept for industry.

Appendix

V1 RPA Chamber Performance Data

```
# Engine name: Vulcan-I 375
# Sat Nov 8 10:31:23 2014
#
#*****************************************************************************************************
# Propellant Specification
#-----------------------------------------------------------------------------------------------------
#    Component  Temp.          Mass           Mole
#                [F]      fraction       fraction
#-----------------------------------------------------------------------------------------------------
#         RP-1   77.0     0.2808989      0.4721131
#        O2(L) -297.4     0.7191011      0.5278869
#-----------------------------------------------------------------------------------------------------
#              Total:     1.0000000      1.0000000
#-----------------------------------------------------------------------------------------------------
#    Exploded formula:  (O)1.056 (C)0.472 (H)0.921
#                O/F:     2.5600000
#              O/F 0:     3.4056663 (stoichiometric)
#              alpha:     0.7516885 (oxidizer excess coefficient)
#-----------------------------------------------------------------------------------------------------
#
# Table 1. Thermodynamic properties
#-----------------------------------------------------------------------------------------------------
#          Parameter       Injector      Nozzle inl      Nozzle thr      Nozzle exi            Unit
#-----------------------------------------------------------------------------------------------------
            Pressure       375.0000        374.3059        216.8203          9.1600             psi
         Temperature      6342.3830       6341.6196       6040.4536       3550.3142               R
            Enthalpy      -338.9768       -339.4829       -628.5813      -1900.2165         Btu/lbm
             Entropy         2.7821          2.7821          2.7821          2.7821       Btu/(lbm·R)
     Internal energy      -885.4791       -885.9123      -1141.5925      -2198.6124         Btu/lbm
Specific heat (p=const)      1.7255          1.7257          1.6695          0.4496       Btu/(lbm·R)
Specific heat (V=const)      1.4579          1.4581          1.4226          0.3656       Btu/(lbm·R)
               Gamma         1.1835          1.1835          1.1735          1.2299
 Isentropic exponent         1.1325          1.1325          1.1290          1.2299
       Gas constant         0.0862          0.0862          0.0849          0.0840       Btu/(lbm·R)
Molecular weight (gas)      23.0469         23.0472         23.3827         23.6280
    Molar mass (gas)         0.0000          0.0000          0.0000          0.0000        bm/lb-mol
  Molar mass (total)         0.0000          0.0000          0.0000          0.0000       lbm/lb-mol
             Density         0.1270          0.1268          0.0782          0.0057          lbm/ft³
      Sonic velocity      3936.4437       3936.1606       3808.1008       3031.2443            ft/s
            Velocity         0.0000        159.1993       3808.1008       8841.7796            ft/s
         Mach number         0.0000          0.0404          1.0000          2.9169
          Area ratio        14.7433         14.7433          1.0000          5.9298
           Mass flux        20.1801         20.1801        297.8310         50.2261       lbm/(ft²·s)
           Viscosity         0.0001          0.0001          0.0001          0.0000        lb/(ft·s)
Conductivity, frozen         0.3593          0.3593          0.3436          0.2088       Btu/(hr·ft·R)
Specific heat (p=const), frozen      0.4855          0.4855          0.4836          0.4496      Btu/(lbm·R)
Prandtl number, frozen       0.6417          0.6417          0.6468          0.6754
Conductivity, effective      1.7100          1.7100          1.5880          0.2088       Btu/(hr·ft·R)
Specific heat (p=const), effective           1.7250          1.7260          1.6690          0.4496      Btu/(lbm·R)
Prandtl number, effective            0.4793          0.4793          0.4832          0.6754
#-----------------------------------------------------------------------------------------------------
#
#-----------------------------------------------------------------------------------------------------
#
```

Table 2. Fractions of the combustion products

Species	Injector mass fract	Injector mole fract	Nozzle inl mass fract	Nozzle inl mole fract	Nozzle thr mass fract	Nozzle thr mole fract	Nozzle exi mass fract	Nozzle exi mole fract
CO	0.3933757	0.3236725	0.3933608	0.3236644	0.3813049	0.3183119	0.3723157	0.3140676
CO2	0.2663994	0.1395082	0.2664230	0.1395224	0.2853858	0.1516286	0.2995192	0.1608069
COOH	0.0000186	0.0000095	0.0000186	0.0000095	0.0000111	0.0000058	0.0000074	0.0000039
H	0.0015864	0.0362728	0.0015863	0.0362719	0.0013729	0.0318490	0.0012220	0.0286469
H2	0.0076524	0.0874880	0.0076523	0.0874872	0.0073869	0.0856830	0.0072104	0.0845129
H2O	0.2450603	0.3135053	0.2450677	0.3135189	0.2532988	0.3287663	0.2590709	0.3397848
H2O2	0.0000114	0.0000077	0.0000114	0.0000077	0.0000068	0.0000047	0.0000045	0.0000031
HCHO,formaldehy	0.0000004	0.0000003	0.0000004	0.0000003	0.0000002	0.0000002	0.0000001	0.0000001
HCO	0.0000184	0.0000146	0.0000184	0.0000146	0.0000103	0.0000083	0.0000067	0.0000054
HCOOH	0.0000020	0.0000010	0.0000020	0.0000010	0.0000012	0.0000006	0.0000008	0.0000004
HO2	0.0000957	0.0000668	0.0000956	0.0000668	0.0000586	0.0000415	0.0000393	0.0000282
O	0.0100983	0.0145465	0.0100963	0.0145438	0.0077331	0.0113018	0.0061716	0.0091143
O2	0.0278003	0.0200230	0.0277968	0.0200207	0.0229897	0.0167995	0.0193503	0.0142883
OH	0.0478804	0.0648835	0.0478703	0.0648707	0.0404396	0.0555989	0.0350809	0.0487373

Table 3. Theoretical (ideal) performance

Parameter	Sea level	Optimum ex	Vacuum	Unit
Characteristic velocity	0.0000	5828.1000	0.0000	ft/s
Effective exhaust velocity	8331.1200	8841.7800	9686.7300	ft/s
Specific impulse (by mass)	258.9400	274.8100	301.0700	lbf·s/lbm
Specific impulse (by weight)	258.9400	274.8100	301.0700	s
Thrust coefficient	1.4295	1.5171	1.6621	

Table 4. Estimated delivered performance

Parameter	Sea level	Optimum ex	Vacuum	Unit
Characteristic velocity	0.0000	5680.5000	0.0000	ft/s
Effective exhaust velocity	7867.8100	8378.4700	9223.4300	ft/s
Specific impulse (by mass)	244.5400	260.4100	286.6700	lbf·s/lbm
Specific impulse (by weight)	244.5400	260.4100	286.6700	s
Thrust coefficient	1.3851	1.4750	1.6237	

#Ambient condition for optimum expansion: H=2.37 mi, p=9.160 psi

Table 5. Altitude performance

Altitude mi	Pressure psi	Effective exhau velocity, ft/s	Specific impulse, s	Thrust coefficient	Thrust lbf
0.0000	14.6959	7867.8130	244.5390	1.3851	699.4050
0.2370	14.0417	7928.1650	246.4150	1.3957	704.7700
0.4750	13.4113	7986.3150	248.2220	1.4059	709.9390
0.7130	12.8041	8042.3260	249.9630	1.4158	714.9180
0.9510	12.2194	8096.2600	251.6390	1.4253	719.7130
1.1880	11.6566	8148.1760	253.2530	1.4344	724.3280
1.4260	11.1150	8198.1320	254.8060	1.4432	728.7690
1.6630	10.5941	8246.1870	256.2990	1.4517	733.0400
1.9010	10.0931	8292.3960	257.7360	1.4598	737.1480
2.1390	9.6116	8336.8140	259.1160	1.4676	741.0970
2.3760	9.1489	8379.4950	260.4430	1.4751	744.8910
2.6140	8.7044	8420.4930	261.7170	1.4824	748.5350
2.8520	8.2777	8459.8580	262.9400	1.4893	752.0350
3.0900	7.8681	8497.6410	264.1150	1.4959	755.3930
3.3270	7.4751	8533.8910	265.2410	1.5023	758.6160
3.5650	7.0982	8568.6570	266.3220	1.5084	761.7060
3.8020	6.7369	8601.9870	267.3580	1.5143	764.6690
4.0400	6.3907	8633.9250	268.3510	1.5199	767.5080
4.2780	6.0590	8664.5170	269.3010	1.5253	770.2280
4.5150	5.7415	8693.8070	270.2120	1.5305	772.8310
4.7530	5.4376	8721.8390	271.0830	1.5354	775.3230

Table 6. Throttled chamber performance

Throttle value	Pressure psi	c ef (SL) ft/s	Is (SL) s	F (SL) lbf	c ef (opt) ft/s	Is (opt) s	F (opt) lbf	c ef (vac) ft/s	Is (vac) s	F (vac) lbf

Appendix A: Figure 1 V1 RPA Chamber Performance Data

V1 RPA Thrust Chamber Size and Geometry Data

```
Vulcan-I 375

Thrust and mass flow rates
------------------------------------------
   Chamber thrust (opt):  744.79984    lbf
 Specific impulse (vac):  286.67287      s
   Chamber thrust (vac):  819.91156    lbf
 Specific impulse (opt):  260.41090      s
   Total mass flow rate:    2.86009  lbm/s
Oxidizer mass flow rate:    2.05670  lbm/s
    Fuel mass flow rate:    0.80340  lbm/s

Geometry of thrust chamber with parabolic nozzle
------------------------------------------
    Dc =    5.03  in       b =   30.00 deg
    R2 =    6.45  in      R1 =    0.98  in
    L* =   59.38  in
    Lc =    6.26  in    Lcyl =    1.04  in
    Dt =    1.31  in
    Rn =    0.25  in      Tn =   16.60 deg
    Le =    3.22  in      Te =   14.94 deg
    De =    3.19  in

  Divergence efficiency:    0.98550
        Drag efficiency:    0.99129
     Thrust coefficient:    1.62370  (vac)
```

Appendix A: Figure 2 V1 RPA Thrust Chamber Size and Geometry Data

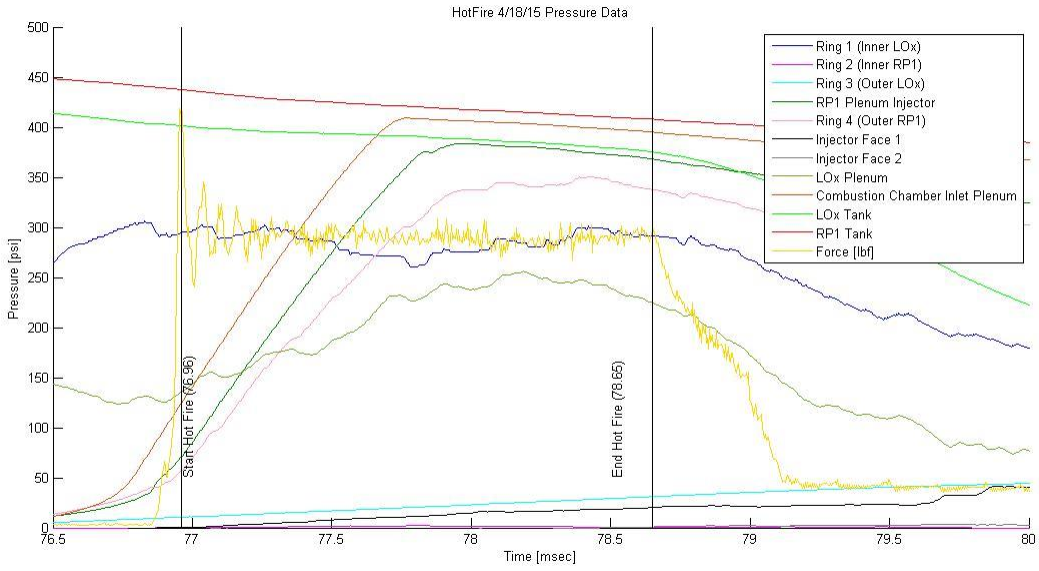

Appendix B: Figure 1 Hot fire 2 Overall Data

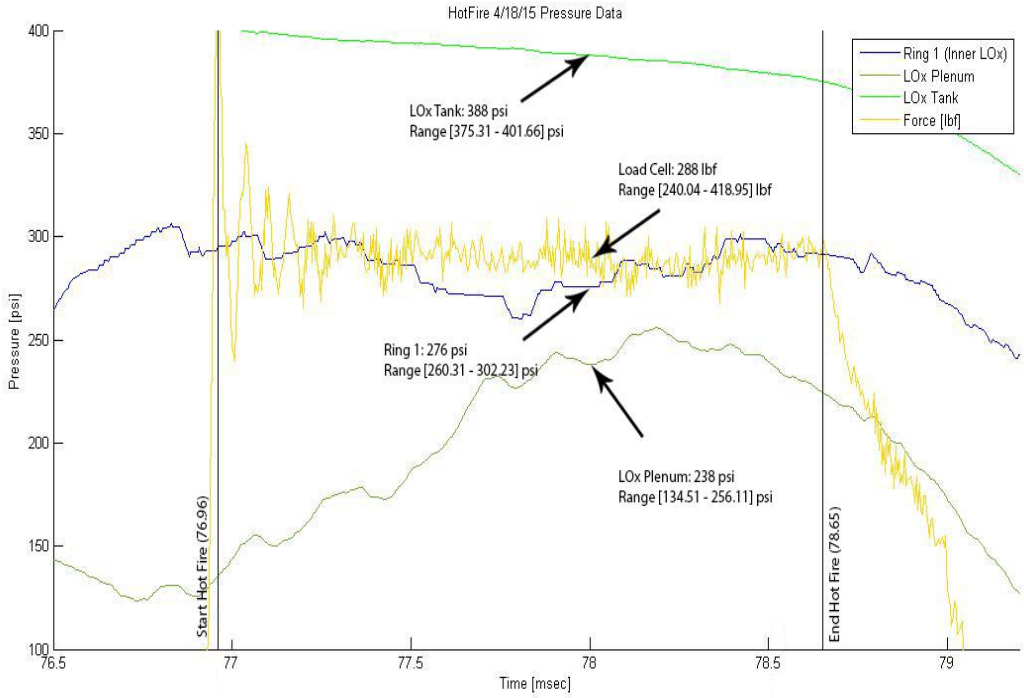

Appendix B: Figure 2 Hot Fire 2 LOx Data

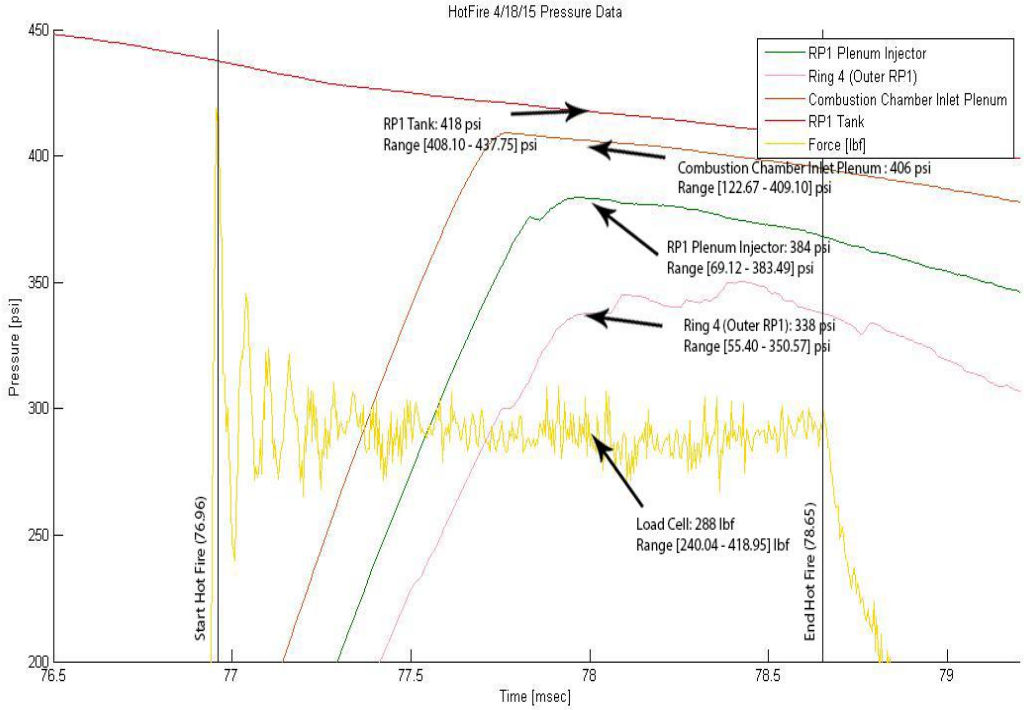

Appendix B: Figure 3 Hot Fire 2 RP1 Data

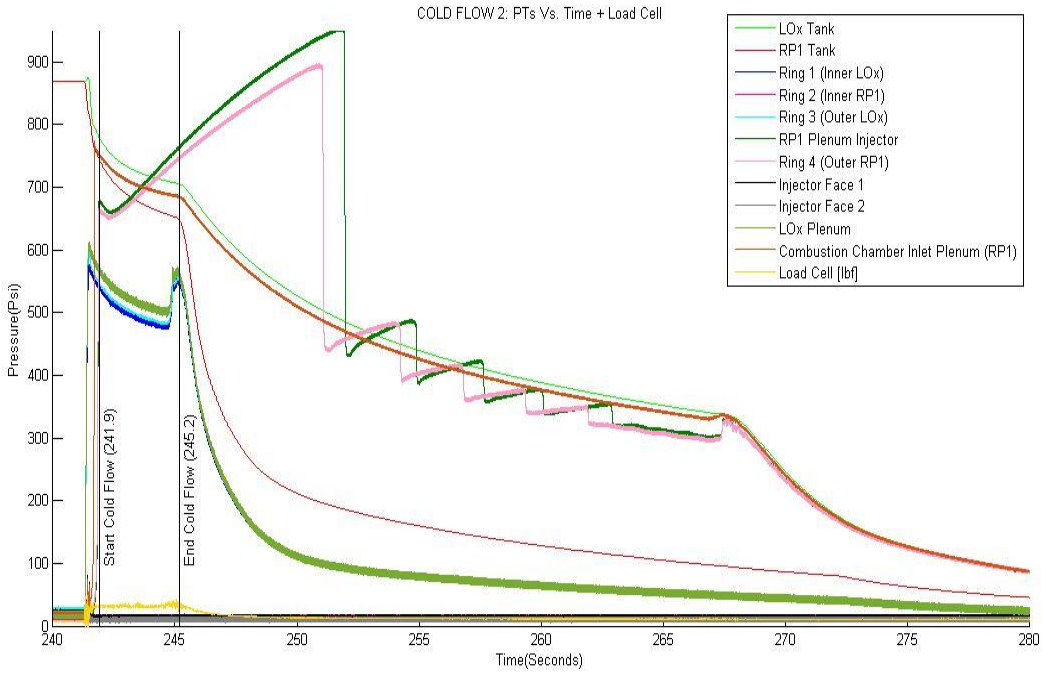

Appendix C: Figure 1 Cold Flow Overall Data

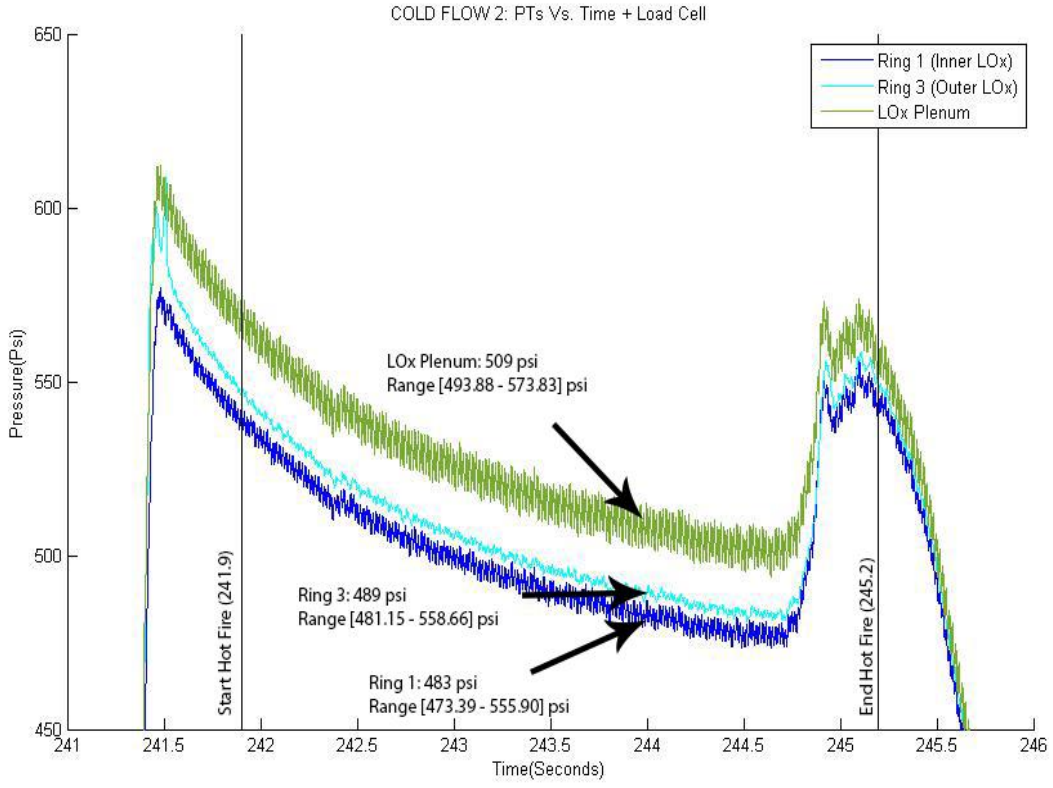

Appendix C: Figure 2 Cold Flow LOx Data

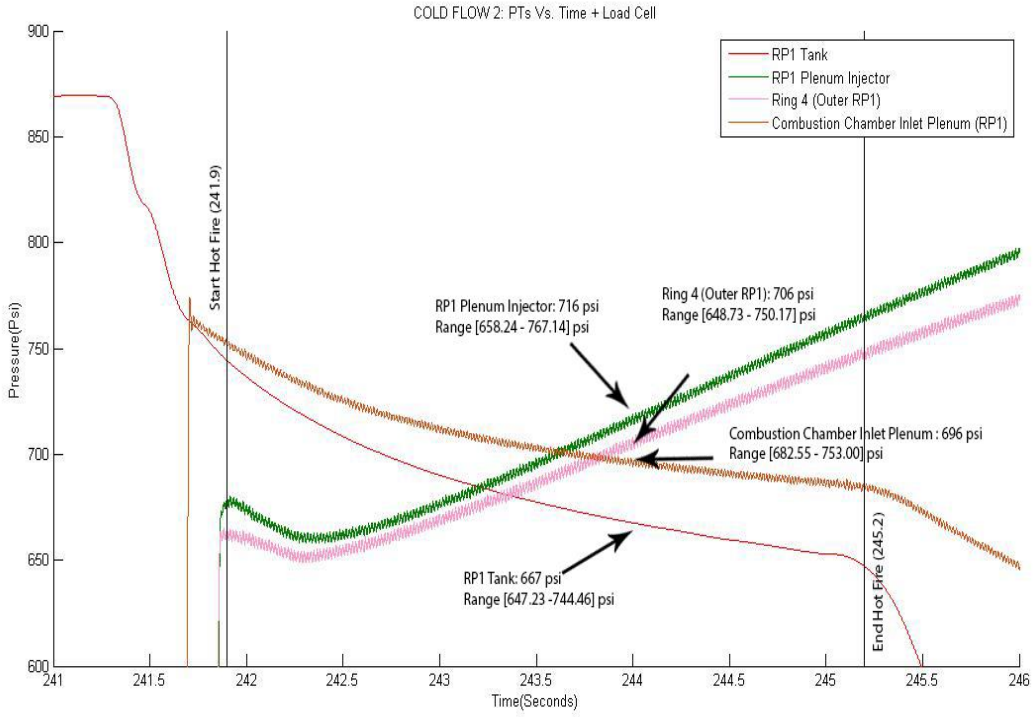

Appendix C: Figure 3 Cold Flow RP1 Data

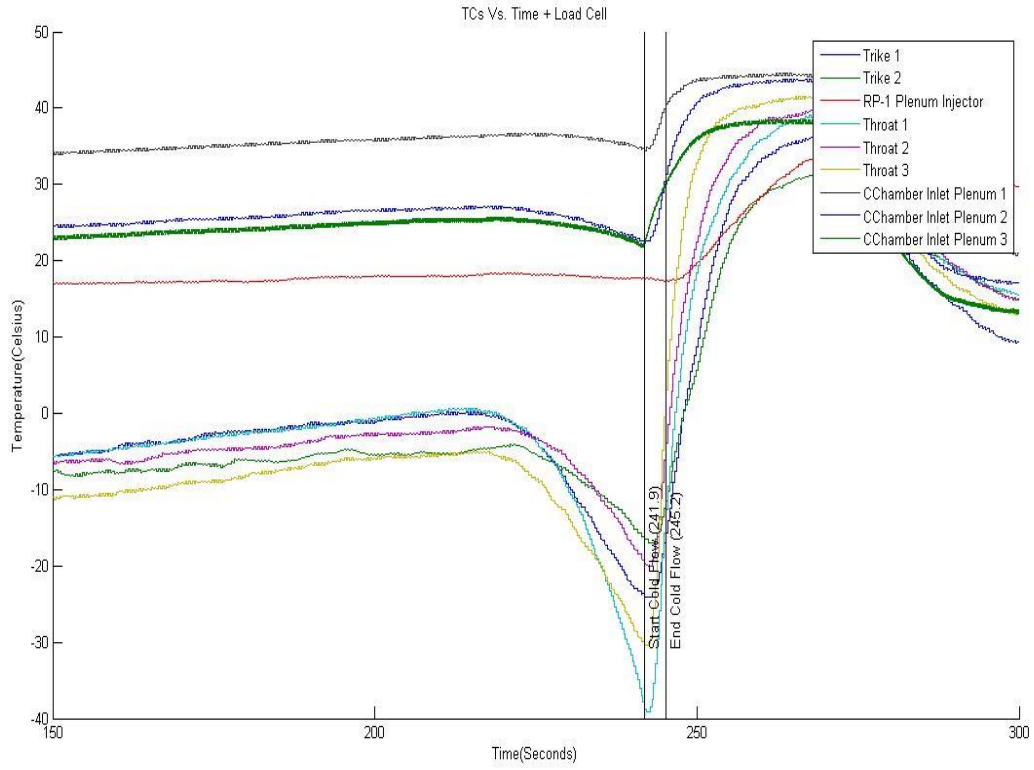

Appendix C: Figure 4 Cold Flow Thermocouple Data

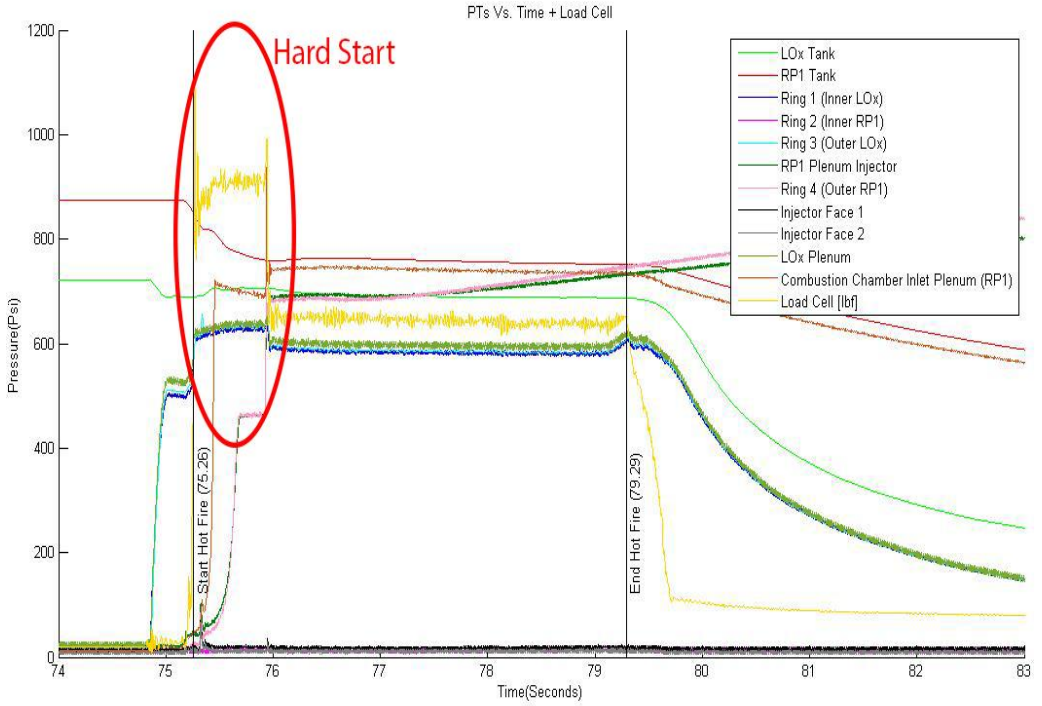

Appendix D: Figure 1 Hot Fire 3 Overall Data

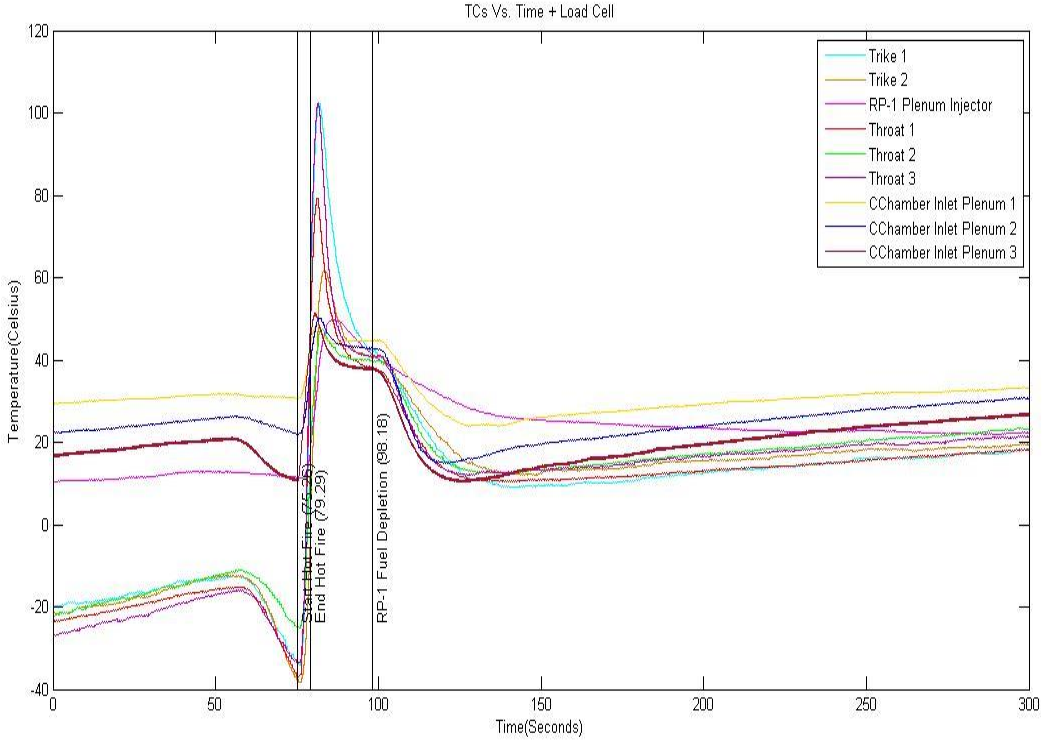

Appendix D: Figure 2 Hot Fire 3 Thermocouple Data

Acknowledgments

D. A. and N. N. Authors would like to thank Dr. Forman Williams for taking his time and using his expertise to help us avoid combustion instability We would also like to thank Jonathan Jones and John Peugeot for logistical and theoretical support when designing this innovative engine. Both Jonathan and John took large amounts of time from their busy schedule to help us start and finish this project. The engine would not have been completed without the help of the engine team comprising of Joshua Benedictos, Alexander Finch, and Johan Arias spending most of their weekends to making sure these designs were correct. In addition to the engine team, we would like to acknowledge the members who took their time to travel and assist with the testing of this engine to obtain the data in this paper. This project would not have been possible without the financial, in-kind, and logistical support from NASA Marshall Space Flight Center, GPI Prototype & Manufacturing Services Inc., Lockheed Martin, The Gordon Center, and XCOR Aerospace to name a few. We lastly would like to thank the Students for the Exploration and Development of Space organization at UC San Diego for having this project be an integral part of the group. All the work in this paper is Patent Pending.

References

[1]"Comprehensive Review of Liquid-Propellant Combustion Instabilities in F-l Engines." PROPULSION AND POWER 9.5 (1993). Print.

[2]Gill, G. S. Liquid Rocket Engine Injectors. Cleveland: National Aeronautics and Space Administration, Lewis Research Center; 1976. Print., Chap. 2

[3]Huzel, Dieter K., and David H. Huang. Modern Engineering for Design of Liquid Propellant Rocket Engines. 2nd ed. Washington, DC: National Aeronautics and Space Administration, 1971, pp 107, Chap. 4

[4]Yang, Vigor. Liquid Rocket Engine Combustion Instability. Washington, D.C.: American Institute of Aeronautics and Astronautics, 1995, Print.

[5]Hill, Philip G., and Carl. R. Peterson. Mechanics and Thermodynamics of Propulsion, 2nd ed. University of Michigan: Addison-Wesley Pub. Co., 1965, Print

[6]Sutton, George P., and Oscar Biblarz. Rocket Propulsion Elements, 8th ed. John Wiley & Sons, 2001. Print

[7]George C. Marshall Space Flight Center, John F. Kennedy Space Center, The Boeing Company Launch Systems Branch, McDonnell Douglas Astronautics Company, International Business Machines Corp. Federal Systems Divisions, Rocketdyne Division North American Rockwell Corp., Space Division North American Rockwell Corp. Saturn V News Reference, Rev 2. Educational Liaison Branch, Public Affairs Office, 1967, Chapter 3 Print

[8]Braeunig, Robert A., Rocket Propulsion, 2012, Online. http://www.braeunig.us/space/propuls.htm

[9]G. J. VanWylen, and R. E. Sonntag, Fundamentals of Classical Thermodynamics, 2nd Ed.; John Wiley & Sons, 1978.

[10]Electro Optical Systems (2014, May). EOS Nickel Alloy IN718 [Material data sheet]. Retrieved from http://gpiprototype.com/images/PDF/EOS_NickelAlloy_IN718_en.pdf